Brazilian Journal
of Chemical
Engineering

ISSN 0104-6632
Printed in Brazil
www.abeq.org.br/bjche

Vol. 28, No. 03, pp. 433 - 446, July - September, 2011

EFFECT OF PARTICLE CLUSTERS ON TURBULENCE MODULATIONS IN LIQUID FLOW LADEN WITH FINE SOLID PARTICLES

Mingjun Pang[1], Jinjia Wei[1*] and Bo Yu[2]

[1]State Key Laboratory of Multiphase Flow in Power Engineering, Xi'an Jiaotong University, Xi'an, 710049, China.
[2]Beijing Key Laboratory of Urban Oil and Gas Distribution Technology, Phone: +86-29-82664462, Fax: +86-29-82669033,
China University of Petroleum, Beijing, 102249, China.
E-mail: jjwei@mail.xjtu.edu.cn

(Submitted: July 22, 2010 ; Revised: November 15, 2010 ; Accepted: March 22, 2011)

Abstract - Studies on particle distributions and interactions between the particles and the liquid turbulence are extremely significant and can help to improve efficiency of industrial processes and final product quality. In this paper, the particle distribution and the particle–turbulence interaction in the solid–liquid flow were investigated in detail by a numerical method. The governing equations of the liquid were solved by direct numerical simulations and the particle was tracked by Newtonian motion equations considering the effects of drag force, lift force, pressure gradient force, and virtual mass force. Two–way coupling was used to explain the effect of the particles on the turbulence. The results showed that the vortex has a great influence on the particle distribution. Most of the particles aggregate at the centre of the channel. Particle clusters along the vortex circumference modulate the development of the vortex. The turbulence modulations showed anisotropy. The Reynolds stress is slightly reduced in a broad range; the energy balance is changed; and an extra term is introduced to maintain a new energy balance.
Keywords: Direct numerical simulation; Particle distribution; Turbulence modulation; Euler–Lagrange model; Two–way coupling.

INTRODUCTION

Many studies have shown that certain additives can greatly modify the turbulence of fluids. It was reported that a dispersed phase such as bubbles and particles in a dilute two–phase flow has a great influence on the turbulent of the carrier phase (Wang *et al*., 1987; Rogers and Eaton, 1991; Tsuji *et al*., 1994; Kaftori *et al*., 1995a, 1995b; Pan and Banerjee, 1996; Kajishima *et al*., 2001; Nagaya *et al*., 2003; Fujiwara *et al*., 2004; Soldati and Marchioli, 2009; etc). Under certain circumstances, some additives (such as polymers, surfactants, micro–bubbles, etc) can even reduce the turbulent frictional drag and energy loss in fluid–transporting processes. In our opinion, these additives can be divided into two major groups according to their physical properties. One is the additives that cannot dissolve in the fluid to form a homogenous and stable phase. This type of additive, which mainly includes micro–bubbles, fine grains, fibers, particles, silts, sands, etc., cannot easily change the rheological properties of the fluid, but can modify the turbulent characteristics of flows when their concentration is low. The other type can dissolve in the fluid to form a stable single–phase solution, simultaneously changing the rheological properties and turbulence structures of the fluids. Commonly, this type of additive includes polymers and surfactants.

In the past, a number of investigations of the additives' modulation on the flow turbulence were performed. It was reported that microbubbles can cause a decrease of the wall–normal turbulence intensity and Reynolds stress of the liquid. The

*To whom correspondence should be addressed

studies showed that the effect of the bubbles on the liquid turbulence is extremely complicated and depends on many factors such as the bubble size and shape, the void fraction, the gas and liquid velocity, the flow direction of the liquid, etc (Nagaya *et al*., 2003; Fujiwara *et al*., 2004; Kitagawa *et al*., 2005; Skudarnov and Lin, 2006; Shawkat *et al*., 2008; etc). For a gas flow laden with solid particles, the studies showed that, for a low mass loading, the micro–particles increase the gas velocity and reduce the turbulent intensities in the wall-normal and spanwise directions. When the mass loading is high, the addition of the micro–particles greatly decreases the velocity, the turbulent intensity, and the Reynolds stress of the gas. The micro–particle influence on the gas turbulence is also associated with many factors, including the particle size and density, the void fraction, the mass loading, etc (Rogers and Eaton, 1991; Tsuji *et al*., 1994; Elghobashi, 1994; Sato and Hishida, 1996; Li and McLaughlin, 2001; Kussin and Sommerfield, 2002; Ferrantea and Elghobashi, 2003; etc). As far as the drag–reducing solutions of polymers and surfactants are concerned, compared to Newtonian fluids, they exhibit many different flow characteristics such as augmentation of the inner boundary layer, an increase of the liquid velocity, a decrease of the wall–normal turbulent intensity and the Reynolds stress, a reduction of turbulent frictional drag, etc. (Kawaguchi, *et al*., 2002; Li and Kawaguchi, 2004; Li *et al*., 2004; Wei *et al*., 2006; etc).

It can be seen from the above review that there are some similarities and differences of the turbulence modulation caused by the different additives of micro size. The obvious common characteristic is that they all reduce the Reynolds stress and the wall–normal turbulent intensity. The biggest difference is that not all of additives can reduce the turbulent frictional drag. In addition, for different additives, the numerical simulation methods are different. For the soluble additives, the numerical simulations are based on the developed constitutive equations of polymers (Yu *et al*., 2004; Tamano *et al*., 2007; etc.). For the insoluble additives, there are three common numerical methods, including the Euler–Euler model, the Euler–Lagrange model, and direct numerical simulations (Loth, 2000; Laín *et al*., 2002).

Compared with gas–solid and gas–liquid two–phase flows, the related reports on the influence of solid particles on liquid turbulence are relatively few, though solid particles can also greatly modify the liquid turbulence. Solid–liquid two–phase flows are frequently observed in many industrial processes and natural phenomena (Kaftori *et al*., 1995a, 1995b; Pan and Banerjee, 1996; Li *et al*., 1999; Kiger and Pan, 2002; Zheng, 2004; Sad–Chemloul and Benrahah, 2008; Muste *et al*. 2009). In particular, cylindrical particles play an important part in the production of composite materials. For example, for a complex material based on chopped fibers, the distribution and orientation of the fibers at the liquid–phase stage, which are closely related to the liquid turbulence structure, directly control the product quality. Thus, it is necessary to study the effects of solid particles on liquid turbulence. Although cylindrical particles are very important for industrial processes, it is very difficult to study the hydrodynamic characteristics of a flow laden with these particles in depth due to the complicated shapes and interfacial forces. To our best knowledge, only a few investigations of this type have been performed (Feng *et al*., 1996; Chiba *et al*., 2001; Lin *et al*., 2004; etc).

In view of the above analysis, we investigated in detail the effect of spherical particles on liquid turbulent with an Euler–Lagrange model. Compared to the Euler–Euler method, the Eulerian–Lagrangian formulation provides a better insight into the particle dynamics, enabling an easy treatment of the particle transients. Unlike previous studies, the effect of particle aggregation behavior on the liquid turbulence is addressed in the present study. We assume that the particle density is equal to that of the fluid, which results in the perfect suspension of the particles in the liquid, and it leads to the fact that the Stokes number of the particles only depends on the particle diameter. The void fraction is less than 10^{-3}, so the interactions between the particles and the particles (wall) can be neglected according to Elghobashi (1994). In order to reduce errors caused by the turbulence model, the liquid velocity is resolved with DNS in the Euler frame of reference, while the particle dynamics are tracked by Newtonian motion equations in the Lagrange frame of reference, including the effects of the drag force, the lift force, the pressure gradient force, and the virtual mass force.

COMPUTATIONAL CONDITION AND METHOD

Computational Condition

The flow domain and the coordinate system are shown in Fig. 1, in which the x, y and z axes correspond to the streamwise, wall–normal and

spanwise directions, respectively. The flow domain size is 10h×2h×5h (=1500×300×750 wall units). Here, h is the channel half–width. The liquid phase is considered to be an incompressible Newtonian fluid. Thermo–physical properties of water at room temperature were adopted. The particle parameters are listed in Table 1, where ρ_p, d_p, M, α_0, Φ, and St denote the particles density, the particle diameter, the total number of particles, the average volume fraction, the average mass loading ($\Phi=\alpha_0\rho_p/\rho_f$), and the Stokes number, respectively. Periodic boundary conditions are adopted in both the streamwise and spanwise directions, and the non–slip condition is imposed at the right and left walls for the liquid phase. Uniform grids are used in the streamwise and spanwise directions. Non–uniform grids are generated by a hyperbolic tangent stretching function and are imposed in the wall–normal direction. Our calculations are based on the friction Reynolds number Re_τ =150, which is calculated from the wall friction velocity u_τ and the channel half width. Initial velocities of the particles are assigned to zero. When a steady turbulence of the liquid is reached, a set of particles is injected into the flow. At the initial time, the particles are introduced into the channel in the following mode. In each x-z plane, the particles are arrayed along the diagonal and each x-z plane contains 300 particles, 300 particles are uniformly distributed at 60 places with an equivalent spacing along the z axis, and each z value is arrayed with five particles. In the channel, totally, there are 65 x-z planes, including the above arraying mode of the particles, and these x-z planes are equivalently inserted in the y direction. The above particle array guarantees that there is the same number of particles corresponding to each y coordinates in the wall-normal direction.

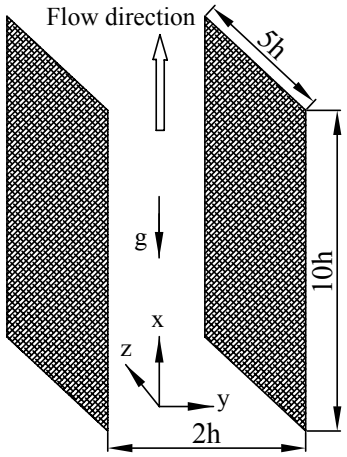

Figure 1: Flow geometry and coordinate system.

Table 1: Parameters of the particles

Parameters	ρ_p/ρ_f	d_p/h	M	α_0	Φ	St
Specific value	1.0	0.011	19200	1.3×10^{-4}	1.3×10^{-4}	0.15

Simulation Overview

Fluid Field

The velocity field of the liquid is calculated by DNS with the incompressible continuity and the Navier–Stokes equations, which can be expressed in the following dimensionless form:

$$\frac{\partial u_{fi}^{+}}{\partial x_i^{*}} = 0 , \tag{1}$$

$$\frac{\partial u_{fi}^{+}}{\partial t^{*}} + u_{fj}^{+}\frac{\partial u_{fi}^{+}}{\partial x_j^{*}} = -\frac{\partial p^{+*}}{\partial x_i^{*}} + \delta_{1i} + \frac{1}{Re_\tau}\nabla^2 u_{fi}^{+} - \overline{f_i^{*}} . \tag{2}$$

The variables associated with length are normalized by the channel half width h, those with velocity dimensions are normalized by the friction velocity u_τ, and these related to the time scale are normalized by h/u_τ. Note that the pressure field is decomposed into a fluctuating kinematic pressure p^{+*} and the average pressure gradient δ_{1i}, which maintains a steady flow against the equilibrium and long–term wall friction produced by both wall boundaries. In Eq. (2), $\overline{f_i^{*}}$ is the local average interfacial force exerted on the fluid by the particles. It is the volume–averaged force of each particle on the surrounding grid points. In the present simulations, $\overline{f_i^{*}}$ is evaluated by

$$\overline{f_i^{*}} = \frac{\rho_p V_p}{\rho_f V}\sum_{j=1}^{M}\left(a_i^{*}\right)_j \tag{3}$$

where V_p, V, a_i^{*} denote the particle volume, the computational domain volume, and the dimensionless acceleration of the particle in the x_i direction.

Equations (1) and (2) are solved by the fractional method. First, the second–order Adams–Bashforth scheme is used to advance the velocity field to an intermediate time without the effect of the pressure gradient:

$$u_{fi}^{+\,n+\frac{1}{2}} = u_{fi}^{+\,n} + \Delta t\left(\frac{3}{2}A_i^{+n} - \frac{1}{2}A_i^{+n-1}\right), \tag{4}$$

where $A_i = \frac{1}{Re}\nabla^2 u_{fi}^+ - u_{fi}^+ \cdot \nabla u_{fi}^+ + f_i^*$, and Δt is the time step. Then, in the second step, $u_{fi}^{+\,n+\frac{1}{2}}$ is corrected by considering the pressure effect:

$$\frac{u_{fi}^{+\,n+1} - u_{fi}^{+\,n+\frac{1}{2}}}{\Delta t^*} = -\nabla p^{+*n+1}. \quad (5)$$

The pressure is solved from the following Poisson equation derived by taking the divergence of Equation (5) and using the continuity Equation (1):

$$\nabla^2 p^{+*n+1} = \frac{1}{\Delta t^*}\nabla \cdot u_{fi}^{+\,n+\frac{1}{2}} \quad (6)$$

After the pressure is solved from Eq. (6), the velocity field for the next time–step can be renewed by Eq. (7). When the effect of the interfacial force is considered, the velocity components for the next time–step are rewritten as

$$u_{fi}^{+\,n+1} = \left\langle u_{fi}^+ \right\rangle - \Delta t^* \frac{\Delta p^{+*\,n+1}}{\Delta x_i^*} + \Delta t^* f_i^*. \quad (7)$$

The divergence form is conservative for the finite–difference schemes when a staggered grid is used. The spatial derivatives are discretized by a second–order central difference scheme. For time integration, the Adams–Bashforth scheme is used for all the terms except that the implicit method is used for the pressure term. This semi–implicit scheme seems to be more suitable for the present cases because of their stability and it is regarded as a standard scheme in the direct numerical simulation. The MAC method is employed to couple the velocity and the pressure fields. The staggered grid system is used to prevent a checker–board pressure field. The Poisson equation for pressure is solved with the multi–grid method.

Additionally, it should be pointed out that the pseudo-spectral method is often preferred because a higher numerical accuracy can be obtained for a given grid size using the pseudo-spectral method than the finite difference method. Thus, many researchers (such as Kim *et al*., 1987; Moster *et al*., 1999; Li *et al*., 2001; etc) have preferred to use the pseudo-spectral method to discretize the spatial terms of the governing equation in DNS. However, Rai and Moin (1991) and Abe *et al*. (2001) pointed out that the finite difference method has the potential to be applied to more complex geometries and spatially developing flow. Therefore, the finite difference method has also been applied to DNS by a number of researchers (such as Rai *et al*., 1991; Gavrilakis *et al*., 1992; Abe *et al*., 2001; Bunner and Tryggvason, 2003; etc). Lu *et al*. (2005) definitively showed that the finite difference method indeed gives results comparable to those produced by the higher-order spectral codes and thus allayed some of the doubts about the use of second-order finite difference methods for turbulence simulations.

Particle Motion

The collisions between the particles are neglected due to the very low global void fraction. In order to simplify the computations, we consider only several important interfacial forces, including the pressure gradient force, the drag force, the added mass force, and the lift force. The motion of the spherical particles in a turbulent field is described by the following simplified equation proposed by Maxey and Riley (1983).

$$\left(C_v + \frac{\rho_p}{\rho_f}\right)\frac{du_{pi}^+}{dt^*} = \frac{Du_{fi}^+}{Dt^*} + \frac{3}{4}\frac{C_D}{d_p^*}\left|u_{fi}^+ - u_{pi}^+\right| \left(u_{fi}^+ - u_{pi}^+\right) + C_v\frac{Du_{fi}^+}{Dt} + C_{LF}\varepsilon_{ijk}\varepsilon_{klm} (u_{fi}^+ - u_{pi}^+)\frac{\partial u_{fl}^+}{\partial x_m^*}. \quad (8)$$

where C_D is the drag coefficient and C_v the added mass coefficient; for spherical particles, C_v=0.5. u_{pi} is the velocity of the particle in the x_i direction, ε the sign of permutation, and C_{LF} the lift coefficient. The drag coefficient is calculated by the following empirical correlation,

$$C_{Di} = \begin{cases} \frac{24}{Re_{pi}} & Re_{pi} \le 1 \\ \frac{24}{Re_{pi}}\left(1 + 0.15\,Re_{pi}^{0.68}\right) & 1 < Re_{pi} < 1000 \\ 0.45 & 1000 \le Re_{pi} < 350000 \end{cases} \quad (9)$$

where Re_{pi} is the ith particle Reynolds number, defined as $Re_{pi} = |u_{fi} - u_{pi}| d_p / v_f$, in which υ_f is the kinematic viscosity of the liquid. The lift coefficient is given by Legendre and Magnaudet (1998) and expressed as

$$C_{LF} = \kappa \frac{9}{4} \sqrt{\left\{C_L^{low\,Re}\left(Re_{pi}, Sr_{pi}\right)\right\}^2 + \left\{C_L^{high\,Re}\left(Re_{pi}\right)\right\}^2}, \quad (10)$$

where

$$C_L^{low\,Re}(Re_{pi}, Sr_{pi}) = \frac{6}{\pi^2}\left(Re_{pi} \cdot Sr_{pi}\right)^{-0.5} \left[\frac{2.255}{\left(1 + 0.2\zeta^{-2}\right)^{1.5}}\right],$$

$$C_L^{high\,Re}\left(Re_{pi}\right) = \frac{1}{2}\left(\frac{1 + 16/Re_{pi}}{1 + 29/Re_{pi}}\right),$$

$$\kappa = 2 - \exp(2.92 d_p^{*2.21}).$$

where Sr_{pi} is the non–dimensional shear rate, $Sr_{pi} = |\omega| d_{pi} / 2|u_{fi} - u_{pi}|$, and $\zeta = \sqrt{Sr_{pi}/Re_{pi}}$.

The momentum response time (τ_p) is the time for the momentum transfer due to drag and is calculated from

$$\tau_p = \frac{\rho_p d_p^2}{18 \mu_f}. \quad (11)$$

The Stokes number of the particles is defined as the ratio of the particle's momentum response time to the characteristic time scale of the carrier fluid

$$St = \frac{\tau_p}{\upsilon_f / u_\tau^2} = \frac{Re_\tau^2}{18}\left(\frac{d_p}{h}\right)^2\left(\frac{\rho_p}{\rho_f}\right). \quad (12)$$

The particle's velocity and displacement are calculated through the integral equation of acceleration by the second order Crank–Nicholson method. A staggered grid system is used to prevent a checkerboard pressure field, which means that the velocity components are located at the cell faces and the other variables are located at the cell centers. Therefore, a three–dimensional 8–node combined with a two–dimensional 4–node Lagrangian interpolation polynomial is used to obtain the velocities of the liquid at the same positions as the particles (near the wall, the interpolation scheme switches to one–sided). Eaton (2009) pointed out that there is little effect of the interpolation scheme on the resulting Lagrangian statistics.

RESULTS AND DISCUSSION

Particle Distribution

The particle distribution plays an important role in the solid–liquid two–phase flow and it has a direct influence on the dynamic characteristics of the two–phase flow and the final sedimentation state of the particles. Just like the fluid field data, 100 files including the coordinates of each particle were saved at equal intervals in the computational process when the change of the probability density function profile of the particle number with the computational time is slight. We performed a statistical average of the particle number corresponding to different positions in the wall–normal direction. The total volume of particles was then divided by the local mesh volume corresponding to different positions in the wall–normal direction. Thus, the profile of the local void fraction can be obtained, as shown in Fig. 2. Fig. 2 shows the profiles of the local void fraction and the particle number across the channel. Here the local void fraction (α) is normalized by the maximum of the local void fraction (α_{max}). It can be seen from Fig. 2 that the particle distribution along the central plane of the channel is almost symmetrical and there are two peak values, which are located near the wall and at the centre of the channel, respectively. The maximum of the void fraction is located at the centre of the channel. Because of the mesh, with a smaller spacing near the wall than at the central part of the channel, the void fraction near the wall is a rather high, even though the particle number is very small. In order to eliminate this effect of the mesh system, the particle number profile independent of the mesh system is presented in Fig. 2(b), which shows that the local number of the particles near the centre of the channel is much greater than that near the wall.

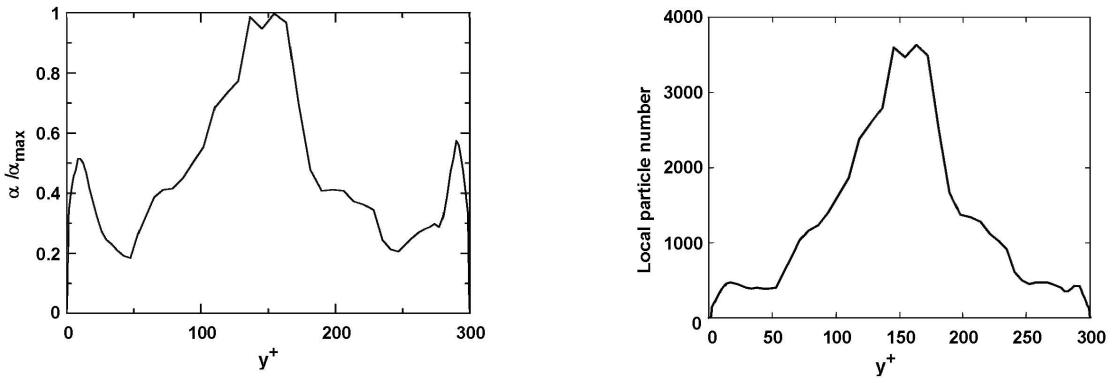

(a) (b)

Figure 2: Local void fraction profile and number of particles along the y direction. (a) Local void of the particles. (b) Particle number profile.

Figure 3 exhibits an instantaneous distribution of the particles in the channel. Fig. 3(b) clearly shows that the particles tend to accumulate near the centre of the channel. This distribution trend is in qualitative agreement with the results given by Alajbegovic *et al*. (1994, 1999) and Hryb *et al*. (2009). Fig. 3 (a) shows an instantaneous profile of the particles and the streamwise velocity of the liquid in the x–z plane at y=0.8h. Note that the particle distribution corresponding to the x axis in the x–z plane depends, to a certain extent, on the initial distribution of the particles, but the initial distribution state of the particles does not influence the motion of the particles along the z axis in the x–z plane. An interesting result is that the particles do not tend to conglomerate in the low speed streaks due to the Stokes number that greatly deviates from 3. This result is in good agreement with the numerical and experimental results of Li *et al*. (1999) and Ling *et al*. (1998). They pointed out that the tendency of the particles to agglomerate into the streaks depends on the particle size and the flow condition. Yamamoto *et al*. (1998) reported that the two–way coupling between the particles and the fluid can reduce the accumulation of the particles in the low speed streaks in the viscous sublayer. Additionally, it can be clearly seen from Fig. 3(c) that the distribution of the particles is very uneven in the y–z plane. Most of the particles accumulate along the circumference of eddies. That might be why the particles tend to move towards the centre of the vortexes under the action of an instantaneous drag force and the high pressure from the surrounding liquid. When these particles move inside the vortexes, they will rotate together with the vortexes. If the motions of the particles along with the vortexes occur under the ideal and perfect condition, these particles might accumulate at the centre of the vortexes. However, these particles, with definite mass, can be influenced by the centrifugal force caused by the rotary motion of the vortexes and escape from the vortexes again. Finally, these particles deposit in the appropriate places at which a balance occurs between the centrifugal force and the interphase force.

In essence, the mechanism responsible for the particle distribution is very complicated and depends on many factors such as the particle diameter, the turbulence structure, the flow direction against gravity, etc. Soldati *et al*. (2009) and Mazumder (2000) pointed out that the coherent motion and the vortex structure play the key role in the particle disposition process near the wall.

Turbulence Statistics of the Liquid Phase

Figure 4 presents the streamwise mean velocity profiles of the liquid and the particles as a function of the wall coordinate, $y^+=yu_\tau/\upsilon_f$. Fig. 4 shows that the present results for the single–phase flow agree fairly well with the well–known law–of–the–wall profile of Newtonian fluids: the linear law $u^+ = y^+$ in the viscous sub–layer ($y^+<5$) and the logarithmic law $u^+ = 2.5\ln y^+ + 5.0$ in the inner layer ($y^+>30$). The streamwise mean velocity of the liquid phase (represented by a dashed line) is higher than that of the single–phase flow in the region of $y^+>10$, and the difference increases with the increase of y^+. One can see from Fig. 3 that a number of particles aggregate along the circumference of the vortex, greatly inhibiting the vortex motion. Thus the velocity fluctuation intensities are reduced, as shown in Fig. 5, in which the turbulence intensities in the wall–normal and spanwise directions are attenuated. This may lead to the fact that part of velocity fluctuation energy is transferred to the mean flow through the interphase force, resulting in an increase of the streamwise mean velocity. The influence of the particles on the liquid velocity is very similar to the numerical results of Pan and Banerjee (1996) for the study condition $d_p^+=2$ and St=0.222.

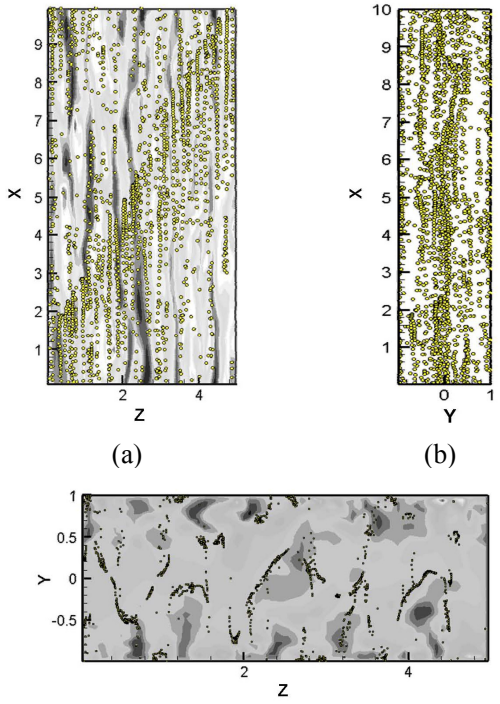

Figure 3: Instantaneous distribution of the particles and streamwise velocity of the liquid. (Flow along the x direction). (a) Distribution in the x–z plane at y=0.8h. (b) Distribution in the x–y plane at z =2.5h. (c) Distribution in the y–z plane at z =5h.

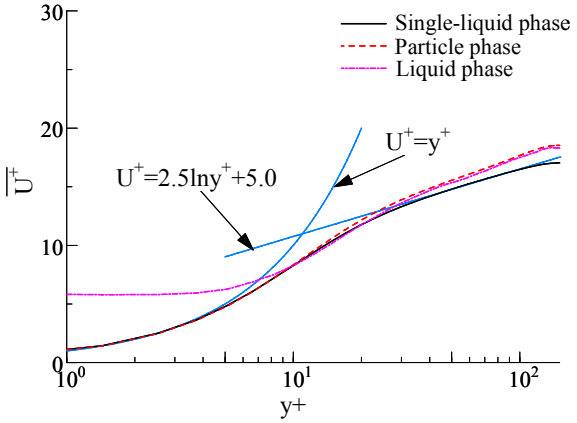

Figure 4: Streamwise mean velocity profiles of the liquid and the particles

As shown in Fig. 4, for the particle–laden flow, the particle velocity is higher than the fluid velocity (i.e., $u_p^+ \geq u_f^+$) in the near–wall region of $y^+<7$ because the particles are free of the wall non–slip condition, while the particles are transported slower than the fluid (i.e., $u_p^+ < u_f^+$) in the region of $7<y^+\leq 100$ due to the back and forth movement of the particles between the high and low velocity regions. Because the Stokes number of the particle (St=0.15) is less than unity in the present study, which implies comparatively good following performance of the particles relative to the carrier phase, the particles almost approach the fluid velocity in the outer region of $y^+ >100$. The velocity distribution trends of the particles and the liquid are in approximate agreement with the results reported by Noguchi and Nezu (2009), which further shows that our computation is correct.

Figure 5 exhibits the profiles of the turbulence intensities along the wall coordinates. For the single–phase flow, the profiles of the turbulence intensities are in good agreement with the DNS data of Yu *et al*. (2004). One can see from Fig. 5 that the turbulence intensities are modified by the particles compared to those for single–phase flow and the modulations of the turbulence intensities take on anisotropy in three directions. The streamwise component remains almost unchanged in the region of $y^+<10$, while it is augmented in a wide central region of the channel. However, the wall–normal and the spanwise components are attenuated in the whole region of the channel. The liquid turbulence modulated by the particles is in qualitative agreement with the results

of Li and Mclaughlin (2001), who investigated the modulation by the particles on gas turbulence employing a numerical method. The effect of the particles on the velocity fluctuation intensities is qualitatively similar to that of a surfactant (Kawaguchi *et al*., 2002; Li and Kawaguchi, 2004; Li *et al*., 2004; Wei *et al*., 2006; etc). However, the underlying mechanisms may be very different. Up to now, the mechanism of carrier–phase turbulence modulated by particles is still not a consensus. Rani *et al*. (2004) considered that the augmentation or attenuation of the streamwise turbulent intensity depends on how the fluid and the particle fluctuations are correlated. If the fluid and the particle velocity fluctuations are positively correlated, the fluid velocity fluctuations are enhanced. That is to say that, if the fluctuating direction of the fluid and the particles is the same and the fluctuation intensity of the particles is higher than that of the fluid, then the fluctuation intensity of the fluid will be enhanced. Otherwise, it will be decreased. In addition, some important conclusions for the turbulence modulation are summarized in Table 2.

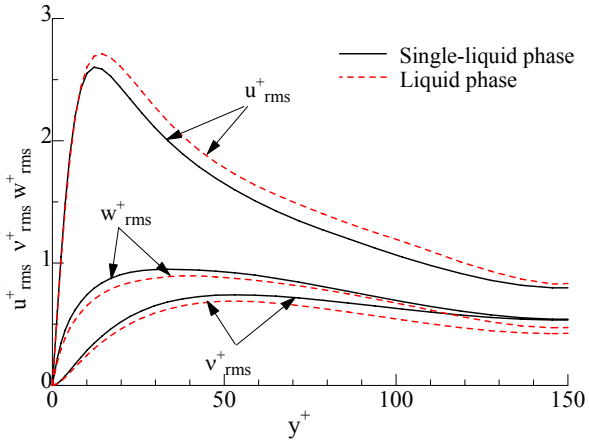

Figure 5: Turbulence intensity profiles.

Table 2: Judgement standard of the turbulence modulation by the particles

Investigators	Important conclusions and judgment standards
Theofanous (1982)	The turbulence production and dissipation depend on the concentration of the particles.
Gore and Crowe (1989)	Whether the turbulence will be augmented or reduced depends on the ratio of d_p/L. Here, d_p is the particle diameter, L the Eulerian length scale. The critical value is $d_p/L \approx 0.1$. If $d_p/L>0.1$, the turbulence is increased. If $d_p/L<0.1$, the turbulence is reduced.
Hetsroni (1989)	The turbulent modulation is related to the critical particle Reynolds number (Re_p). The particles with $Re_p>400$ would augment the turbulence due to vortex shedding behind the particles, and those with $Re_p<400$ would attenuate it.
Yuan and Michaelides (1992)	The acceleration of the particles in the vortexes is responsible for the turbulence reduction, and the flow velocity disturbance due to the wake flow or the vortices shed behind the particles is considered to be the main mechanism responsible for the turbulence enhancement. Combination of both processes results in the turbulent modulation.
Yarin and Hetsroni (1994)	The particle–turbulence interaction is related to the particle size. The fine particles lead to the turbulence attenuation and the coarse particles caused the turbulence increase. The turbulence modulation depends on the total mass content of the fluid–particle mixture, the density ratio, the particle Reynolds number, and the ratio of the particle size to the turbulence length scale.
Elghobashi (1994)	The particle–turbulence interaction is related to the void fraction, the ratio of the response time (τ_b) of the particles to the Kolmogorov time scale (τ_K), and the ratio of the response time of the particles to the turnover time of the large eddy (τ_e). The detailed content can be seen in the following table.
Noguchi and Nezu (2009)	The particle–turbulence interaction depends on the ratio of the particle diameter (d_p) to the Kolmogorov microscale length (η). If $d_p>\eta$, the addition of particles will enhance the turbulence of the carrier phase; if $d_p<\eta$, the turbulence will be attenuated.

$10^{-6}<\alpha_0<10^{-3}$			
τ_b/τ_K		τ_b/τ_e	
$(10^{-2},10^{2})$	$(10^{2},10^{4})$	$(10^{-4},10^{0})$	$(10^{0},10^{2})$
enhance dissipation	enhance production	enhance dissipation	enhance production

In our opinion, if the particle size, the void fraction, and the density are very small, the momentum exerted by the particles on the fluid is not sufficient enough to change the mean flow. However, the momentum of the particles may be enough to alter the local velocity of the fluid at the location of the particle, which will result in changes of the fluctuation intensities even if the mean velocity remains unchanged. This implies that the fluctuation intensities are more susceptible to the effect of the particles than the mean velocity. If the momentum produced by the particles bridges the gap between the mean velocity and the instantaneous velocity of the local fluid, the fluctuation intensities will be attenuated. Otherwise, they will be enhanced. The momentum of the particles acting on the fluid is associated with many factors, such as the characteristics of the flow field, the computational accuracy of the interphase action forces, the density ratio of the fluid to the particle, the particle Reynolds number, the initial conditions of the fluid and particle, the particle size and shape, the void fraction, etc. Therefore, to achieve a quantitative and reasonable description, a great number of investigations should be performed in the future.

Figure 6 shows the budget of shear stress for the liquid phase and the single–liquid phase. For the single–phase flow, the total shear stress is equal to the sum of the viscous shear stress and the Reynolds shear stress. For the single-phase flow, the profiles of the stress components are in good agreement with the results of Yu *et al*. (2004). The stress balance relation can be expressed as follows:

$$\tau_{total} = 1 - \frac{y^+}{Re_\tau} = -\overline{u'^+ v'^+} + \frac{1}{Re_\tau}\frac{\partial u^+}{\partial y^*}. \qquad (13)$$

Compared with the single–phase liquid, the Reynolds stress ($-\overline{u'^+ v'^+}$) of the liquid phase is slightly reduced in a broad region of the channel by the addition of the particles. In addition, the peak position is a little farther from the wall than that of the single–liquid phase. Compared with the Reynolds stress, the viscous stress changes slightly. The reduction of the Reynolds stress might result from a decorrelation between the velocity fluctuation components, u' and v'. For the dilute two–phase flow, the total shear stress still conforms to the linear distribution along the width of the channel. When a steady state is reached, the following balance equation is satisfied:

$$\tau_{total} = 1 - \frac{y^+}{Re_\tau} = -\overline{u'^+ v'^+} + \frac{1}{Re_\tau}\frac{\partial u^+}{\partial y^*} + \int_{y^*}^{1} \overline{f_i^*}\, dy^* . \qquad (14)$$

In Eq. (14), the right–hand terms denote the non–dimensional Reynolds stress, the viscous stress, and the interphase stress, respectively. Compared with the single–phase flow, there is one additional term, called the interphase stress, that maintains the total balance. The mutual interactions between the particles and the liquid are realized through the interphase momentum exchanged by the interphase stress. In the present study, the interphase stress reduces the turbulence intensities in the wall–normal and the spanwise directions and enhances the mean flow.

The budget of the turbulence kinetic energy is presented in Fig. 7. It can be seen from Fig. 7 that the trends of all terms for the budget of the turbulence kinetic energy are essentially the same for the single–phase and two–phase flows. However, from the quantitative point of view, there are some differences between them. Compared with the single–liquid phase, there is an extra term called the interphase force term that maintains the energy balance in the liquid phase, which represents the energy transferred from the continuous phase to the particles. In the present study, the interphase force term is less than zero and thus it represents a dissipation term. This means that the addition of the particles leads to an extra dissipation. According to the turbulence modulation criteria presented by Noguchi and Nezu (2009), this phenomenon will occur only if the diameter of the particles is less than the Kolmogorov microscale length.

In the present study, the computational domain in wall units was 1500×300×750. A grid with grid dimensions of 64×64×64 was adopted. The grid spacing of Δy^+ ranged from about 0.45 near the wall to 9 at the center of the channel in wall units. In the x and z directions, the grid spacing was Δx^+=23.4 and Δz^+=11.72 in wall units, respectively. The particle diameter in wall units was d_p^+=1.65. The Kolmogorov length was calculated by the following expression:

$$\eta^+ = \left(\frac{\nu^3}{\varepsilon}\right)^{1/4}\frac{u_\tau}{\nu} = \left(\frac{u_\tau^4}{\varepsilon\nu}\right)^{1/4} = \frac{1}{\left(\varepsilon^+\right)^{1/4}}. \qquad (15)$$

For the present simulation, ε^+ varied from 0.19 near the wall to 0.033 at the center of the channel, as shown in Fig. 7. The computation shows that the Kolmogorov length scale (η^+) in wall units has the smallest value of about 1.52 near the wall and the largest value of 4.17 at the center of the channel. It is very clear that the grid size in the wall-normal direction is smaller than the Kolmogorov length scale in the near-wall region and comparable to the Kolmogorov length scale in the centre region. Thus, the grid size can capture the smallest eddy size. In our study, the Kolmogorov time scale in wall units has the smallest value of 2.29 ν/u_τ^2 near the wall and the largest value of 5.50 ν/u_τ^2 at the center of the channel. However, our time step size used was 0.015 ν/u_τ^2, which is much smaller than the Kolmogorov time scale. Therefore, the resolution of the DNS is guaranteed. Further detailed validation for the present DNS can be found in the literature (Yu *et al*., 2004).

The above analysis shows that the particle diameter is slightly greater than the Kolmogorov length in a small region near the wall, but is smaller than that in a broad central region of the channel. According to Noguchi and Nezu (2009), the turbulence should be attenuated near the wall but strengthened at the centre of the channel. On the whole, the turbulence should be reduced along the width of the channel. The above analysis shows that our results adhere to their standard fairly well. Additionally, it should be pointed out that the extra dissipation caused by the interphase force includes two parts: one is the real dissipation, i.e., the turbulent energy that is turned into heat through the frictional interaction between the particles and the fluid; the other is the pseudo–dissipation, namely, the turbulent energy that is transferred to the mean flow through the interaction between the particle clusters and the vortices, which reduces the velocity fluctuations. If the former is larger than the latter, the addition of the particles will increase the friction drag. Otherwise, as shown in our study, the friction drag is reduced and the flow rate is enhanced due to the addition of the particles.

In order to understand the turbulence modulations, the budget terms of the Reynolds normal stress $\overline{u'^+ u'^+}$ are analyzed, as shown in Figs. 8 and 9. The trends of all terms are almost the same, but there are some slight differences between the single–liquid phase and the liquid phase. In effect, the particle changes the energy balance relationship and introduces a new term to maintain the energy balance. The pressure gradient term of the normal stress $\overline{u'^+ u'^+}$ is plotted in Fig. 9 to emphasize the difference between the single–liquid phase and the liquid phase. Fig. 9 shows that the energy lost by the pressure strain is reduced in the region of $y^+<45$, in contrast with the single–liquid phase. This means that the energy transferred from $\overline{u'^+ u'^+}$ to $\overline{v'^+ v'^+}$ and $\overline{w'^+ w'^+}$ is reduced by the addition of the particles, which leads directly to the reduction of the velocity fluctuation in the wall–normal and spanwise directions because the cross–flow gains less energy from the bulk flow.

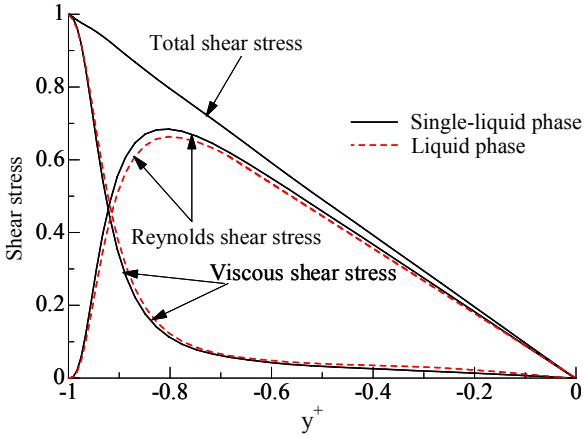

Figure 6: Budget of shear stress.

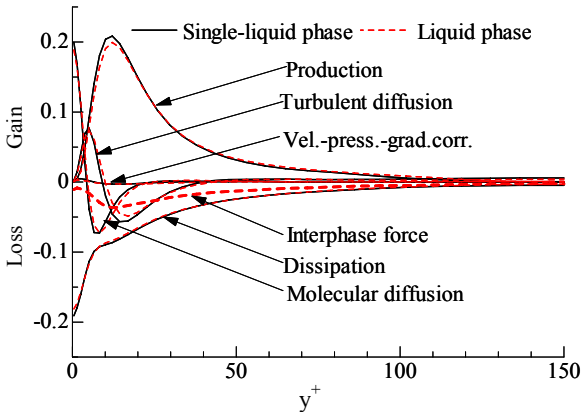

Figure 7: Budget of turbulence kinetic energy.

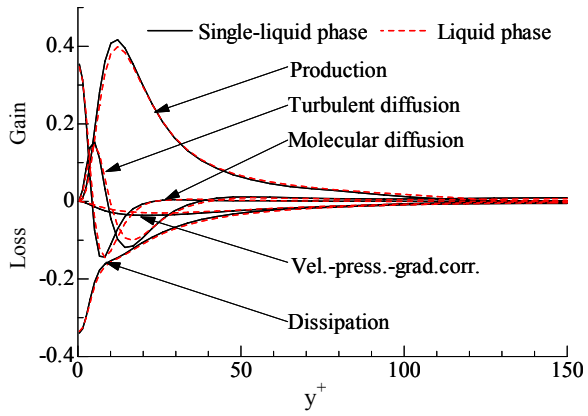

Figure 8: Budget of Reynolds stress $\overline{u'^{+}u'^{+}}$

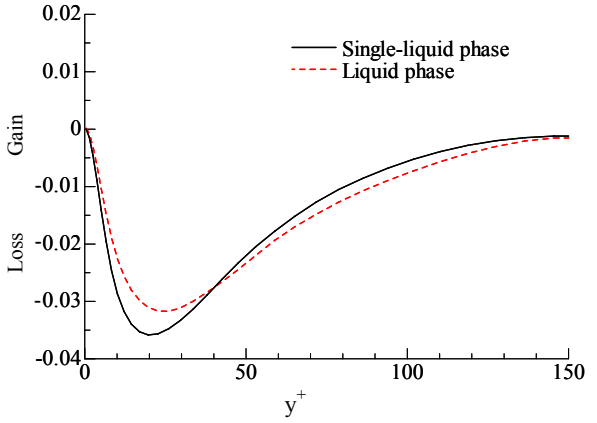

Figure 9: Profiles of pressure gradient term of $\overline{u'^{+}u'^{+}}$

Overview of the Modulation of the Particles on the Fluid Turbulence

Although a number of experimental and numerical investigations of the modulation of the fluid turbulence by particles have been performed, the perfect mechanism responsible for the turbulence modulation has still not been developed. Kim *et al*. (2005) considered that, when there is no change in the volume of the dispersed flows, which include the bubbly flow, the droplet flow, and the particle–laden flow, the turbulent production and dissipation of the continuous phase can be understood by similar mechanisms. Some judgement standards of the turbulent modulation by the particles are summarized in Table 2. It can be seen from Table 2 that different researchers presented different standards to predict or judge the turbulence modulation by the addition of the particles. Up to now, there is not a physical model that can explain all physical phenomena. Some conclusions are even in contradiction with the experimental results of the literature. For example, the turbulent energy enhancement by the particles is attributed to the presence of the particle wakes. However, Hardalupas *et al*. (1989) proved experimentally that particles without wakes (small Re_p) can also increase the production of the turbulent energy. Yarin and Hetsroni (1994) showed that the ratio of the particle diameter to the turbulence scale does not generalize the experimental data for all flows laden with particles of different sizes. Additionally, the experimental work of Noguchi and Nezu (2009) showed that the particle–fluid interaction is governed by the Kolmogorov microscale rather than the macroscale such as the integral scale in sediment–laden flows. Although our numerical results support the physical standard presented by Noguchi and Nezu (2009), there is still lots of work to do to further check and verify the accuracy and correctness of the conclusion.

CONCLUSIONS

In this paper, a dilute solid–liquid two–phase flow in a channel was investigated by the Euler–Lagrange model. The present particle diameter is small and the particle density is the same as that of the fluid. The Stokes number (St =0.15) is less than unity, so that the particle follows the fluid motion well. Direct numerical simulations were performed for the fully developed single–liquid and solid–liquid two–phase turbulent flows. The coupling between the phases was considered by regarding the interphase force as a momentum source term of the continuous phase. The distribution of the particles and the turbulence modulation of the liquid were analyzed in detail. The following conclusions can be drawn:

1) Most of particles move closer to the centre of the channel; the local void fraction and the number of particles exhibit an approximately symmetric distribution along the central plane of the channel; the maximum appears at the center of the channel.

2) Particles accumulate along the circumference of eddies in the y–z plane. However, they show an even distribution in the x–z plane. The vortex has the greatest influence on aggregation of the particles.

3) Particle clusters formed along the circumference of the vortex inhibit the vortex motion, which leads to turbulence modulation of the liquid. The turbulence intensity is enhanced in the streamwise direction and is weakened in the other two directions. The Reynolds stress is slightly reduced along the width of the channel and the flow

rate of the liquid is slightly increased. The results show that the influence of particle clusters on the turbulence modulation is very different from the influence of single particles on it.

4) The particles change the energy balance relation and an extra dissipation term is introduced to maintain the energy balance; our results validate the physical model presented by Noguchi and Nezu (2009) that, when the particle diameter is less than the Kolmogorov microscale length, the addition of the particle will increase the turbulence dissipation.

ACKNOWLEDGEMENTS

We gratefully acknowledge the financial support from the NSFC Fund (No. 51076124, 50823002, 50821064, 50876114), the Specialized Research Fund for the Doctoral Program of Higher Education of China (No. 20090201110002), Jiangsu Provincial Natural Science Foundation (BK2009145), and the Fundamental Research Funds for the Central Universities.

REFERENCES

Abe, H., Kawamura, H., Matsuo, Y., Direct Numerical Simulation of a Fully Developed Turbulent Channel Flow With Respect to the Reynolds Number Dependence. ASME Journal of Fluids Engineering, 123, No 6, 382 (2001).

Alajbegovic, A., Assad, A., Bonetto, F., Lahey Jr, R. T., Phase distribution and turbulence structure for solid/fluid upflow in a pipe. International Journal of Multiphase Flow, 20, No 3, 453 (1994).

Alajbegovic, A., Drew, D. A., Lahey Jr., R. T., An analysis of phase distribution and turbulence in dispersed particle/liquid flows. Chemical Engineering Communication, 174, No 1, 85 (1999).

Bunner, E., Tryggvason, G., Effect of bubble deformation on the properties of bubbly flows. Journal of Fluid Mechanics, 495, 77 (2003).

Chiba, K., Yasuda, K., Nakamura, K., Numerical solution of fiber suspension flow through a parallel plate channel by coupling flow field with fiber orientation distribution. Journal of Non–Newtonian Fluid Mechanics, 99, No 2-3, 145 (2001).

Eaton, J. K., Two–way coupled turbulence simulations of gas–particle flows using point–particle tracking. International Journal of Multiphase Flow, 35, No 9, 792 (2009).

Elghobashi, S., On Predicting Particle–Laden Turbulent Flows. Applied Scientific Research, 52, No 4, 309(1994).

Feng, J., Huang, P. Y., Joseph, D. D., Dynamic simulation of sedimentation of solid particles in an Oldroyd–B fluid. Journal of Non–Newtonian Fluid Mechanics, 63, No 1, 63 (1996).

Ferrantea, A., Elghobashi, S., On the physical mechanisms of two–way coupling in particle–laden isotropic turbulence. Physics of Fluids, 15, No 2, 315 (2003).

Fujiwara, A., Minato, D., Hishida, K., Effect of bubble diameter on modification of turbulence in an upward pipe flow. International Journal of Heat and Fluid Flow, 25, No 3, 481 (2004).

Gavrilakis, S., Numerical simulation of low-Reynolds-number turbulent flow through a straight square duct. Journal of Fluid Mechanics, 244,101 (1992).

Gore, R. A., Crowe, C. T., Effect of particle size on modulating turbulent intensity. International Journal of Multiphase Flow, 15, No 2, 279 (1989).

Hardalupas, Y., Taylor, A. M. K. P., Whitelaw, J. H., Velocity and particle flux characteristics of turbulent particle–laden jets. Proceedings of the Royal Society of London. Series A, Mathematical and Physical Sciences, 426, No 1870, 31 (1989).

Hetsroni, G., Particle–turbulence interaction. International Journal of Multiphase Flow, 15, No 5, 735 (1989).

Hryb, D., Cardozo, M., Ferro, S., Goldschmit, M., Particle transport in turbulent flow using both Lagrangian and Eulerian formulations. International Communications in Heat and Mass Transfer, 36, No 5, 451 (2009).

Hu, H. H., Patankar, N. A., Zhu, M. Y., Direct numerical simulations of fluid–solid systems using the arbitrary Lagrangian–Eulerian technique. Journal of Computational Physics, 169, No 2, 427 (2001).

Kaftori, D., Hetsroni, G., Banerjee, S., Particle behavior in the turbulent boundary layer. I. motion, deposition, and entrainment. Physics of Fluids, 7, No 5, 1095 (1995a).

Kaftori, D., Hetsroni, G., Banerjee, S., Particle behavior in the turbulent boundary layer. II. velocity, and distribution profiles. Physics of Fluids, 7, No 5, 1107 (1995b).

Kajishima, T., Takiguchi, S., Hamasaki, H., Miyak,e Y., Turbulence structure of particle–laden flow in a vertical plane channel due to vortex shedding. JSME International Journal Series B, 44, No 4, 526 (2001).

Kawaguchi, Y., Segawa, T., Feng, Z., Li, P., Experimental study on drag–reducing channel flow with surfactant additives–spatial structure of turbulence investigated by PIV system. International Journal of Heat and Fluid Flow, 23, No 5, 700 (2002).

Kiger, K. T., Pan, C., Suspension and turbulence modification effects of solid particulates on a horizontal turbulent channel flow. Journal of Turbulence, 3, No 2, 019 (2002).

Kim, J., Moin, P., Moser, R. D., Turbulence statistics in fully developed channel flow at low Reynolds number. Journal of Fluid Mechanics, 177, 133 (1987).

Kim, S., Bock Lee, K., Gu Lee, C., Theoretical approach on the turbulence intensity of the carrier fluid in dilute two–phase flows. International Communications in Heat and Mass Transfer, 32, No 3-4, 435 (2005).

Kitagawa, A., Hishida, K., Kodama, Y., Flow structure of microbubble–laden turbulent channel flow measured by PIV combined with the shadow image technique. Experiments in Fluids, 38, No 4, 466 (2005).

Kussin, J., Sommerfeld, M., Experimental studies on particle behaviour and turbulence modification in horizontal channel flow with different wall roughness. Experiments in Fluids, 33, No 1, 143 (2002).

Laín, S., Bröder, D., Sommerfeld, M., Göz, M. F., Modelling hydrodynamics and turbulence in a bubble column using the Euler–Lagrange procedure. International Journal of Multiphase Flow, 28, No 8, 1381 (2002).

Legendre, D., Magnaudet, J., The lift force on a spherical bubble in a viscous linear shear flow. Journal of Fluid Mechanics, 368, 81 (1998).

Li, C., Mosyak, A., Hetsroni, G., Direct numerical simulation of particle–turbulence interaction. International Journal of Multiphase Flow, 25, No 2, 187 (1999).

Li, F. C., Kawaguchi, Y., Investigation on the characteristics of turbulence transport for momentum and heat in a drag–reducing surfactant solution flow. Physics of Fluids, 16, No 9, 3281 (2004).

Li, F. C., Kawaguchi, Y., Hishida, K., Investigation on the characteristics of turbulence transport for momentum and heat in a drag–reducing surfactant solution flow. Physics of Fluids, 16, No 9, 3281 (2004).

Li, Y. M., Mclaughlin J. B., Numerical simulation of particle–laden turbulent channel flow. Physics of Fluids, 13, No 10, 2957 (2001).

Lin, J. Z., Zhang, W. F., Sheng, Y. Z., Numerical research on the orientation distribution of fibers immersed in laminar and turbulent pipe flows. Journal of Aerosol Science, 35, No 1, 63 (2004).

Ling, W., Chung, J. N., Troutt, T. R., Crowe, C. T., Direct numerical simulation of a three–dimensional temporal mixing layer with particle dispersion. Journal of Fluid Mechanics, 358, 61 (1998).

Loth, E., Numerical approaches for motion of dispersed particles, droplets and bubbles. Progress in Energy and Combustion Science, 26, No 3, 161 (2000).

Lu, J. C., Fernández, A., Tryggvason, G., The effect of bubbles on the wall drag in a turbulent channel flow. Physics of Fluids, 17, No 9, 095102 (2005).

Maxey, M. R., Riley., J. J., Equation of motion for a small rigid sphere in a non–uniform flow. Physics of fluids, 26, No 4, 883 (1983).

Mazumder, R., Turbulence–particle interactions and their implications for sediment transport and bedform mechanics under unidirectional current: some recent developments. Earth–Science Reviews, 50, No 1-2, 113 (2000).

Moser, R. D., Kim, J., Mansour, N. N., Direct numerical simulation of turbulent channel flow up to Re_τ=590. Physics of Fluids, 11, No 4, 943 (1999).

Muste, M., Yu, K., Fujita, I., Ettema, R., Two–phase flow insights into open–channel flows with suspended particles of different densities. Environmental Fluid Mechanics, 9, No 2, 161 (2009).

Nagaya, S., Hishida, K., Kakugawa, A., Kodama, Y., PIV/LIF measurement of wall turbulence modification by microbubbles. Proceedings of the 4th International Symposium on Smart Control of Turbulence, Tokyo, Japan, pp. 69-78 (2003).

Noguchi, K., Nezu, I., Particle turbulence interaction and local particle concentration in sediment–laden open–channel flows. Journal of Hydro–environment Research, 3, No 2, 54 (2009).

Pan, Y., Banerjee, S., Numerical simulation of particle interactions with wall turbulence. Physics of Fluids, 8, No 10, 2733 (1996).

Rai, M. M., Moin, P., Direct simulation of turbulent flow using finite-difference schemes. Journal of Computational Physics, 96, No 1, 15 (1991).

Rani, S. L., Winkler, C. M., Vanka, S. P., Numerical simulations of turbulence modulation by dense particles in a fully developed pipe flow. Powder Technology, 141, No 1-2, 80 (2004).

Rogers, C. B., Eaton, J. K., The effect of small particles on fluid turbulence in a flat–plate,

turbulent boundary layer in air. Physics of Fluids A, 3, No 5, 928 (1991).

Sad–Chemloul, N., Benrahah, O., Measurement of velocities in two–phase flow by laser velocimetry: interaction between solid particles' motion and turbulence. ASME Journal Fluids Engineering 130, No 7, 071301 (2008).

Sato, Y., Hishida, K., Transport process of turbulence energy in particle–laden turbulent flow. International Journal of Heat and Fluid Flow, 17, No 3, 202 (1996).

Shawkat, M. E., Ching, C. Y., Shoukri, M., Bubble and liquid turbulence characteristics of bubbly flow in a large diameter vertical pipe. International Journal of Multiphase Flow, 34, No 8, 767 (2008).

Skudarnov, C. X., Lin, C. X., Drag reduction by gas injection into turbulent boundary layer: Density ratio effect. International Journal of Heat and Fluid Flow, 27, No 3, 436 (2006).

Soldati, A., Marchioli, C., Physics and modelling of turbulent particle deposition and entrainment: Review of a systematic study. International Journal of Multiphase Flow, 35, No 9, 827 (2009).

Tamano, S., Itoh, M., Hoshizaki, K., Yokota, K., Direct numerical simulation of the drag–reducing turbulent boundary layer of viscoelastic fluid. Physics of Fluids, 19, No 7, 075106 (2007).

Theofanous, T. G., Sullivan, J., Turbulence in two–phase dispersed flows. Journal of Fluid Mechanics, 116, 343 (1982).

Tsuji, Y., Tanaka, T., Yonemura, S., Particle induced turbulence. Applied Mechanics Review, 47, No 6, S75 (1994).

Wang, S. K., Lee, S. J., Jones Jr, O. C., Lahey Jr, R. T., 3–D turbulence structure and phase distribution measurements in bubbly two–phase flow. International Journal of multiphase flow, 13, No 3, 327 (1987).

Wei, J. J., Kawaguchi, Y., Yu, B., Feng, Z. P., Rheological characteristics and turbulent friction drag and heat transfer reductions of a very dilute cationic surfactant solution. Journal of Heat Transfer, 128, No 10, 977 (2006).

Yamamoto, Y., Tanaka, T., Tsuji, Y., LES of gas–particle turbulent channel flow (the effect of inter–particle collision on structure of particle distribution). The Third International Conference on Multiphase Flow, Lyon, France (1998).

Yarin, L. P., Hetsroni, G., Turbulence intensity in dilute two–phase flows–3 The particles– turbulence interaction in dilute two–phase flow. International Journal of Multiphase Flow, 20, No 1, 27 (1994).

Yu, B., Li, F. C., Kawaguchi, Y., Numerical and experimental investigation of turbulent characteristics in a drag–reducing flow with surfactant additives. International Journal of Heat and Fluid Flow, 25, No 6, 961 (2004).

Yuan, Z., Michaelides, E. E., Turbulence modulation in particulate flows–a theoretical approach. International Journal of Multiphase Flow, 18, No 5, 779 (1992).

Zheng, Y., Radial particle profiles in a liquid–solid CFB with varying viscosity. Chemical Engineering & Technology, 27, No 3, 769 (2004).